INSTITUTE OF PHYSICS PUBLISHING JOURNAL OF PHYSICS B: ATOMIC, MOLECULAR AND OPTICAL PHYSICS

J. Phys. B: At. Mol. Opt. Phys. **39** (2006) 3983–3991 doi:10.1088/0953-4075/39/18/026

Angularly resolved electron wave packet interferences*

K Varjú[1], P Johnsson[1], J Mauritsson[1,2], T Remetter[1], T Ruchon[1], Y Ni[3], F Lépine[3], M Kling[3], J Khan[3], K J Schafer[2], M J J Vrakking[3] and A L'Huillier[1]

[1] Department of Physics, Lund University, PO Box 118, SE-221 00 Lund, Sweden
[2] Department of Physics and Astronomy, Louisiana State University, Baton Rouge, LA 70803-4001, USA
[3] FOM-Institute AMOLF, Kruislaan 407, 1098 SJ Amsterdam, The Netherlands

E-mail: anne.lhuillier@fysik.lth.se

Received 6 April 2006, in final form 29 June 2006
Published 12 September 2006
Online at stacks.iop.org/JPhysB/39/3983

Abstract

We study experimentally the ionization of argon atoms by a train of attosecond pulses in the presence of a strong infrared laser field, using a velocity map imaging technique. The recorded momentum distribution strongly depends on the delay between the attosecond pulses and the laser field. We interpret the interference patterns observed for different delays using numerical and analytical calculations within the strong field approximation.

(Some figures in this article are in colour only in the electronic version)

1. Introduction

The rapid advances made in the performance of light sources and detection techniques allow us to investigate and control states of matter in ever finer detail. Light sources, with wavelengths ranging from the infrared (IR) to the extreme ultraviolet (XUV), are becoming increasingly coherent, intense, well characterized and controllable. The shortest available light pulses are now significantly shorter than 1 fs [1, 2], thus offering a unique tool for studies of ultrafast electron dynamics. At the same time, new spectroscopic techniques have been developed which allow determination of the momenta in three dimensions of several interacting particles [3, 4], providing a detailed knowledge of interaction processes.

In a recent letter [5], we studied the angular and energy-resolved electron emission from argon atoms exposed to a train of attosecond pulses in the presence of a strong IR laser field at an intensity of 2.5×10^{13} W cm^{-2}. The three-dimensional dynamics of the electron wave packet was investigated using a velocity map imaging technique [6]. We found a striking variation of the angular distributions as a function of the timing of the electron wave packet's injection into the continuum relative to the phase of the IR laser field. In particular, we

* This article is a late contribution to the special issue containing papers from the 10th International Conference on Multiphoton Processes, published in July 2006.

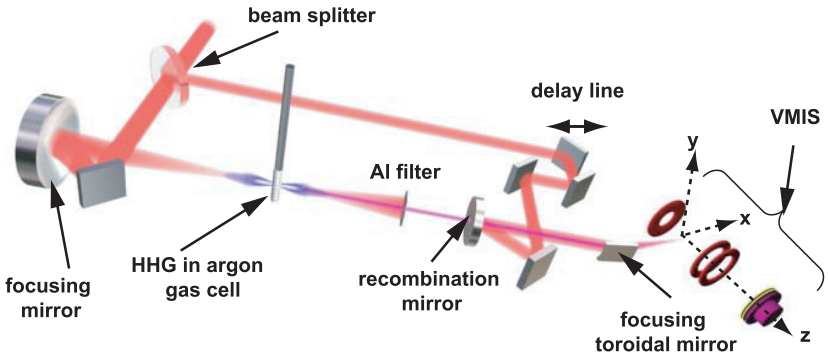

Figure 1. Experimental setup. In one arm of a Mach–Zehnder interferometer, part of a 800 nm laser beam generates high-order harmonics in a cell filled with argon. The harmonics are subsequently spatially and spectrally filtered using a hard aperture and a 200 nm Al filter. The remaining IR field travelling in the other arm of the interferometer is recombined with the attosecond pulse train after reflection on a spherical convex mirror with a hole, which lets through the XUV pulses. Both XUV and IR fields are refocused with a toroidal mirror into the sensitive region of a velocity map imaging spectrometer.

observed clear interferences between wave packets created at a given time and those created half an IR cycle later. We showed that for certain delays, information on the phase of the electron wave packets can be extracted in a way resembling lateral-shearing interferometry for optical wavefronts [7]. The present paper is a follow-up of [5], intending to give a more complete description of the experiments as well as a detailed analytical description of the structure of the interference patterns.

2. Experimental method and results

2.1. Experimental setup

Our experimental setup is schematized in figure 1. The attosecond pulses are synthesized from harmonics generated by focusing 35 fs, 1.6 mJ IR laser pulses into a 3 mm long argon gas cell at 30 mbar pressure. A 200 nm thick aluminium filter allows us to eliminate the fundamental field, spectrally filter out the low-order harmonics and partially compensate for the positive intrinsic chirp of the attosecond pulses [2, 8]. Characterization of the attosecond pulses is done by the RABITT (reconstruction of attosecond beating by interference of two-photon transitions) technique [9]. Since this characterization technique uses an ionization signal, it is actually the electron wave packets created by ionization that are characterized, and from which the temporal and spectral properties of the light pulses are determined [10]. In our experiment, we create a train of electron wave packets from argon with an individual duration of 200 as, a central kinetic energy of 11 eV and a bandwidth of 11 eV.

The dressing IR pulse is a fraction (500 μJ) of the laser beam, finely delayed with a piezo-electric actuated translation stage relative to the XUV pulses. It is superposed to the XUV beam after reflection on a convex mirror (see figure 1). Both beams are then focused by a toroidal platinum mirror into the active region of a velocity map imaging spectrometer (VMIS), crossing a beam of noble gas atoms (see figure 2). The IR and XUV fields are both linearly polarized along the y-axis (see figure 2) and are perpendicular to the detection axis of the VMIS (z-axis in figure 2).

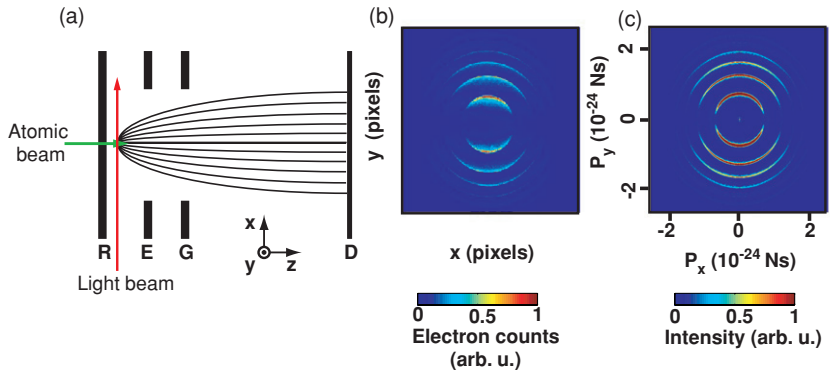

Figure 2. (a) Principle of the velocity map imaging technique. Electrons are extracted with a repeller (R) and an extractor (E) and collected by a detector (D) (G = ground). (b) Experimental raw data obtained in helium using high-order harmonics generated in argon. (c) 2D cut through the 3D momentum distribution, obtained after inversion.

Electrons created in the interaction region are accelerated by a dc electric field towards imaging microchannel plates coupled to a phosphor screen. The coordinates where electrons impact on the detector provide a measurement of two of the three velocity components of the ejected electrons. The third velocity component (along the dc electric field axis, i.e. the z-axis) is not explicitly measured, but has the same distribution as the component of the velocity perpendicular to the polarization axis of the experiment, the latter being chosen in the plane of the detector, i.e. along the y-axis. The three-dimensional momentum distribution at a given delay between the XUV and IR fields is recovered by inversion of the measured projection (figure 2(b)) using an iterative procedure [11]. The concentric rings obtained in figure 2(c) are due to ionization from the different odd harmonics (from the 17th to the 23rd) leading to electrons with increasing kinetic energies from the inner ring to the outer ring.

2.2. *Experimental results*

In figure 3, we show experimental results obtained in argon ionized by a train of attosecond pulses in the presence of a strong laser field with an intensity of 2.5×10^{13} W cm^{-2}, for different delays between the two fields. The cartoons below the panels indicate the time-dependent vector potential (**A**) of the IR field, polarized along the y-direction, together with the sequence of attosecond pulses for the corresponding delays. The momentum distributions are found to be strongly dependent on this delay. We note the following features for the different delays.

(i) The electrons are located on circles centred at the origin as a result of the interference between electron wave packets separated by one laser cycle. This can be expressed in either the time or frequency domain. In the time domain, the interference fringes arise from the repetition frequency of the process. In the frequency domain, the total energy absorbed by the atom is always an integral number times the frequency of the fundamental of the Ti:sapphire laser (since the harmonics are multiples of this laser).

(ii) There is an additional interference structure superimposed on the previous one, which appears as two sets of concentric circles, symmetrically off-centred with respect to the x-axis. One of these sets is illustrated by white circles in figure 3. Their centre varies along the p_y axis as a function of the delay. In figure 4(a), the position of the centre of these circles along the p_y axis is plotted as a function of the XUV/IR delay.

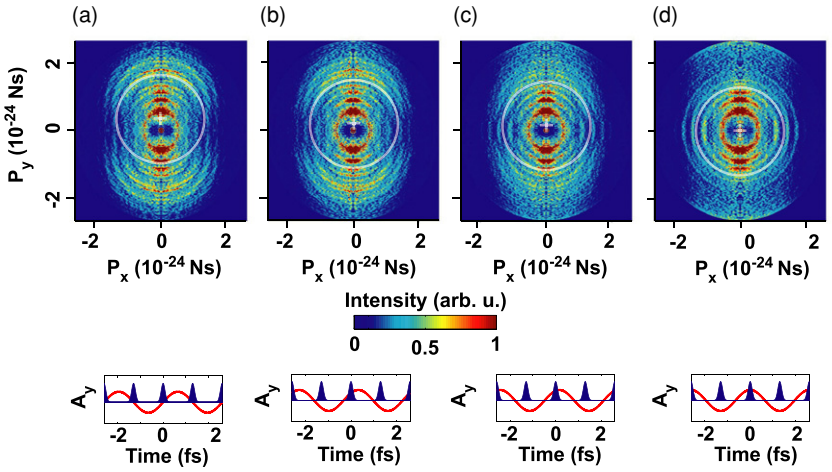

Figure 3. Experimental photoelectron momentum distributions from ionization of argon for different delays (depicted in the cartoons) between the attosecond pulses and the IR laser field (a)–(d).

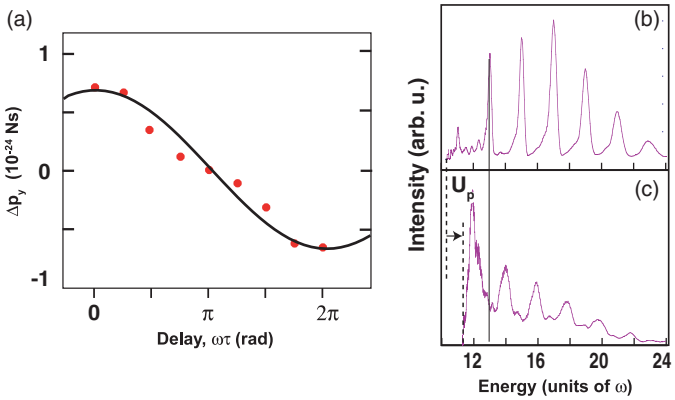

Figure 4. Analysis of the experimental data. (a) Centre of the circles outlined in white in figure 3 as a function of delay. (b) Photoelectron spectrum along the p_y axis due to harmonics only. (c) Lineout of the interference pattern along the p_x axis in figure 3(d).

(iii) From figure 3(a) to 3(d), the momentum distribution becomes more and more elongated, with an increased yield of high-energy electrons (some of them outside the observation window). This effect has been observed in previous experiments [1, 12].

(iv) A striking interference pattern appears as the delay varies from (a) to (d) on the p_x axis. A lineout along the p_x axis is presented in figure 4(c) and compared to photoelectron spectra obtained with only harmonics (figure 4(b)). In general, the kinetic energy of the photoelectrons is given by

$$E_c = \frac{p^2}{2m} = n\hbar\omega - I_p - U_p, \tag{1}$$

where n is an integer, I_p is the ionization energy and U_p is the ponderomotive energy ($= e^2E^2/4m\omega^2$, approximately equal to 1.5 eV in our experiment). The abscissa in

figures 4(b) and (c) is chosen to be the total energy absorbed in units of the IR photon energy ω. Interestingly, the maxima of the interference pattern in figure 4(c) correspond to an even multiple of ω.

To interpret these features and discuss their implication, we develop a theoretical model based on the strong field approximation (SFA) [13].

3. Theoretical interpretation

To understand the experimental results in detail, we describe the photoionization of an atom by an XUV field in the presence of an IR laser field. The transition amplitude from the ground state is approximated by [13, 14]

$$a_{\mathrm{p}}(\tau) = -\mathrm{i}\int_{-\infty}^{+\infty} \mathbf{E}_{\mathrm{XUV}}(t)\cdot\mathbf{d}[\mathbf{p}+e\mathbf{A}(t+\tau)]\,\mathrm{e}^{-\mathrm{i}S(t,\tau)/\hbar}\,\mathrm{d}t, \tag{2}$$

where $\mathbf{p}$ is the final momentum, $\mathbf{E}_{\mathrm{XUV}}(t)$ is the XUV field and $\mathbf{A}(t+\tau)$ is the IR vector potential, delayed by τ relative to the attosecond pulses. The phase accumulated by an electron ionized at time t in the IR field is given by the quasi-classical action

$$S(t,\tau) = \int_{t}^{+\infty} \frac{(\mathbf{p}+e\mathbf{A}(t'+\tau))^2}{2m}\,\mathrm{d}t' - I_{\mathrm{p}}t. \tag{3}$$

3.1. Numerical calculations

We first calculate the momentum distribution due to ionization by a single attosecond pulse. The dipole moment is approximated by

$$\mathbf{d}(\mathbf{p}) = \frac{\mathbf{p}}{(\mathbf{p}^2+2I_{\mathrm{p}})^3}, \tag{4}$$

to simulate ionization of an s-electron [13]. The momentum distribution obtained with a 160 as pulse centred at 37 eV is shown in figure 5(a). At a delay such that the attosecond pulse coincides with the zero of the vector potential, the momentum distribution is barely affected even though the ionization takes place in the presence of an IR laser field. When an IR laser field at an intensity of 2×10^{13} W cm^{-2} is added with a delay such that the attosecond pulse coincides with the maximum or minimum of the vector potential, the momentum distribution is shifted upwards (figure 5(c)) or downwards. The electron created with an initial momentum $\mathbf{p}_{\mathrm{i}}$ exchanges additional momentum with the laser field equal to $-e\mathbf{A}$, $\mathbf{A}$ being the vector potential at the time of ionization and $-e$ the electron charge; it thus ends up in a final continuum state characterized by the momentum $\mathbf{p} = \mathbf{p}_{\mathrm{i}} - e\mathbf{A}$.

In figures 5(d)–(f), we use a sequence of two attosecond pulses, separated by half the IR laser period. In general, the IR field will introduce a (delay-dependent) momentum shift (i.e. a *shear*) between consecutive electron wave packets that will lead to interferences in the region of the momentum space where the wave packets overlap. In addition, there is a difference in the accumulated phase between consecutive wave packets, which originates from the different dynamics of the electron in the laser field depending on $\mathbf{A}$ at the time of ionization. Figure 5(f) is the result of the coherent superposition of two momentum distributions shifted in opposite directions. In the region of overlap, i.e. along the p_x axis, a strong interference pattern appears. In figures 5(d) and (e), the momentum distributions coincide and the interference structure is due to the difference in accumulated phase between the two electron wave packets. The IR field introduces an asymmetry in this accumulated phase, leading to interference fringes that are off-centre in figure 5(e) (see also the white circles in figure 3).

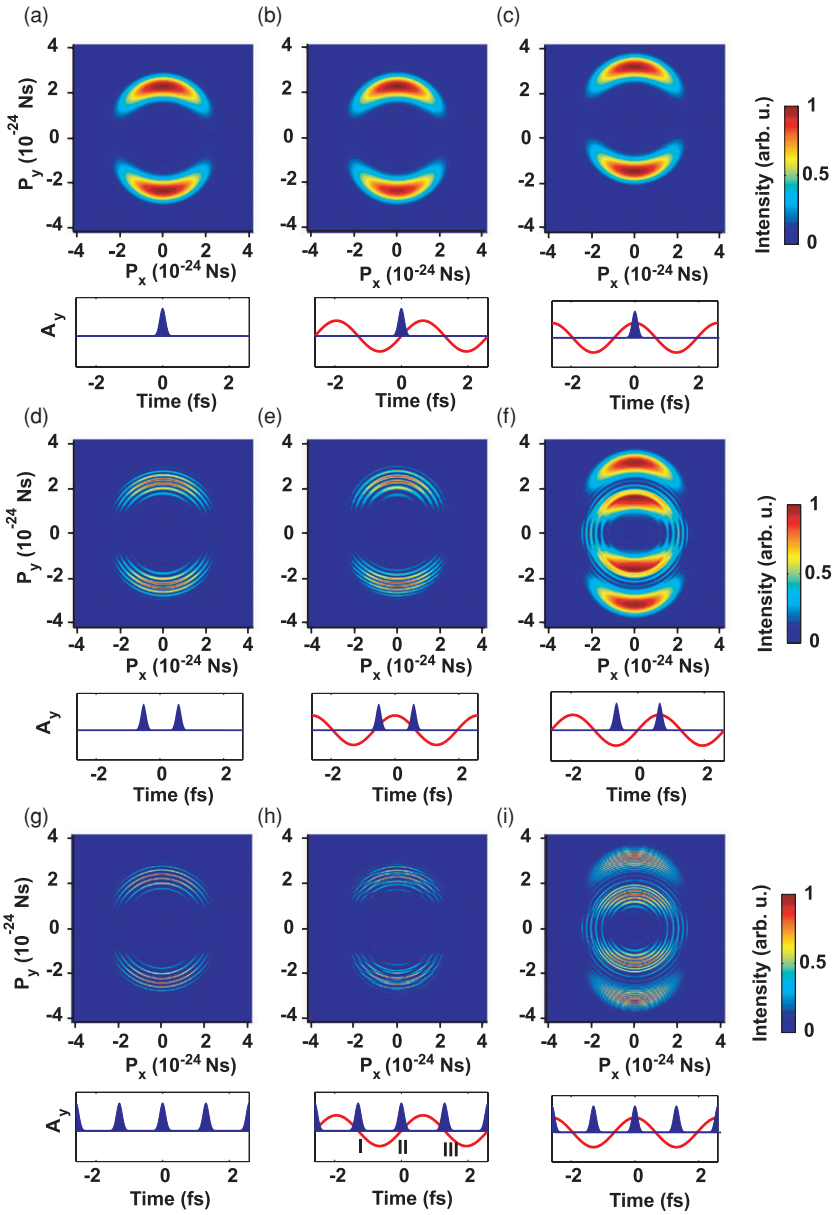

Figure 5. Numerical simulations within the strong field approximation. (a) Ionization by a single attosecond pulse. (b) and (c) In the presence of an IR laser field such that the attosecond pulse coincides with a zero (b) or a maximum (c) of the corresponding vector potential. (d) Ionization by two attosecond pulses separated by half the IR period. (e) and (f) In the presence of an IR laser field. (g)–(i) Ionization by a train of attosecond pulses. The cartoons depict the relative delay between the attosecond pulses and the IR field.

Finally, in figures 5(g)–(i), we use a train of attosecond pulses. As expected, the interference fringes become sharper (figure 5(g)). In figure 5(h), the complex structure is due to three sets of interference fringes, one centred at the origin and two centred on either the positive or negative sides of the p_y axis. These are due to interferences between electron

wave packets such as (I, III), (I, II) and (II, III), respectively (as labelled in the figure). In figure 5(i), the two lobes on the top and bottom of the image contain interferences between electron wave packets that are produced with a delay of one full optical cycle with respect to each other and with the same sign of the vector potential (see e.g. contributions I and III below figure 5(h)). The central structure in the image contains extensive interference contributions between electron wave packets that are produced on consecutive half-cycles of the laser and with an opposite sign of the vector potential (see e.g. wave packet pairs (I, II) and (II, III)). Compared to figures 5(d)–(f), the additional repetition due to the train of pulses leads to an additional interference structure centred on the origin which covers the whole momentum distribution. The interference pattern in the overlap region in figure 5(i) remains clearly visible, becoming even sharper than that in figure 5(f).

It should be noted that the finite duration of the attosecond pulses tends to blur some of the interference patterns, especially the off-centred circles that move with the delay. However, for the pulses used in this work for both the experiments and the calculations, this effect remains small and all the features discussed above are clearly seen in the figures. Thus, as shown in the next section, the main features can be readily found using the limit of ultrashort pulses.

3.2. Analytical calculations for ultrashort pulses

In the limit of a train of ultrashort attosecond pulses, we can analytically determine the position of all the interference structures discussed above. Let us express the XUV field as a sum of phase-locked odd harmonics with constant amplitude, or alternatively in the time domain as a train of Dirac-like pulses, only contributing at times $t = k\pi/\omega$:

$$E_{\mathrm{XUV}}(t) \approx \sum_{q\ \mathrm{odd}} \mathrm{e}^{\mathrm{i}q\omega t} \approx \sum_{k} (-1)^k \delta\left(t - \frac{k\pi}{\omega}\right). \tag{5}$$

The transition amplitude becomes

$$a_{\mathrm{p}}(\tau) \approx \sum_{k} (-1)^k d_y[\mathbf{p} + (-1)^k e\mathbf{A}(\tau)] \exp\left(-\mathrm{i}S\left(\frac{k\pi}{\omega}, \tau\right) \Big/ \hbar\right), \tag{6}$$

with

$$S\left(\frac{k\pi}{\omega}, \tau\right) = -\left(\frac{\mathbf{p}^2}{2m} + U_{\mathrm{p}} + I_{\mathrm{p}}\right)\frac{k\pi}{\omega} + \frac{U_{\mathrm{p}}}{2\omega}\sin(2\omega\tau) - \frac{eA_0 p_y}{m\omega}(-1)^k \cos(\omega\tau), \tag{7}$$

where we assume that $\mathbf{A}(t+\tau) = \mathbf{A}_0 \sin[\omega(t+\tau)]$. The interference pattern is determined by the phase difference between two consecutive electron wave packets $(k+1, k)$

$$\Delta\Phi_k = \pi + \Delta\phi_k - \frac{\Delta S_k}{\hbar}, \tag{8}$$

where

$$\Delta\phi_k = \arg[d_y(\mathbf{p} + (-1)^{k+1} e\mathbf{A}(\tau))] - \arg[d_y(\mathbf{p} + (-1)^k e\mathbf{A}(\tau))] \tag{9}$$

and

$$\Delta S_k = \left(\frac{\mathbf{p}^2}{2m} + U_{\mathrm{p}} + I_{\mathrm{p}}\right)\frac{\pi}{\omega} + (-1)^k \frac{2eA_0 p_y}{m\omega}\cos(\omega\tau). \tag{10}$$

Let us introduce the total energy absorbed by the atom: $W = \mathbf{p}^2/2m + U_{\mathrm{p}} + I_{\mathrm{p}}$. Equation (8) simplifies when the attosecond pulses coincide with maxima/minima or zero crossings of the vector potential. When the attosecond pulses coincide with the zeros of the vector potential, i.e. $\tau = 0$, then

$$\Delta\Phi_k = \pi - \frac{W\pi}{\hbar\omega} - (-1)^k \frac{2eA_0 p_y}{m\hbar\omega}. \tag{11}$$

The position of the maxima of the interference pattern between two consecutive wave packets is then given by

$$W = (2n+1)\hbar\omega - (-1)^k \frac{2eA_0 p_y}{m\pi}, \tag{12}$$

which can be written as

$$\frac{1}{2m}\left[p_x^2 + \left(p_y + (-1)^k \frac{2eA_0}{\pi}\right)^2\right] = (2n+1)\hbar\omega - 0.19U_\mathrm{p} - I_\mathrm{p}. \tag{13}$$

In momentum space, this corresponds to concentric circles that are centred around $(0, (-1)^k 2eA_0/\pi)$ and separated in energy by $2\hbar\omega$. The position of the centre of the interference fringes enables one to determine the absolute magnitude of the vector potential of the IR field. For other delays, the centre of the interference fringes varies according to $2eA_0\cos(\omega\tau)/\pi$, as illustrated in figure 4(a). The experimental measurements follow well this theoretical prediction.

When on the other hand, $\tau = \pi/2$,

$$\Delta\Phi_k = \pi - \frac{W\pi}{\hbar\omega} + \Delta\phi_k. \tag{14}$$

In this case, there is no difference in the accumulated phase, but the IR field induces a shear in the momentum distribution: different initial momentum states are made to overlap by the momentum transfer and information on the relative phase between different momenta states of the initial electron wave packet can be deduced, as shown in [5]. The fact that the interference fringes are located at the position of the even harmonics in figure 4(c) indicates that the initial momentum amplitude distribution changes sign across the $p_y = 0$ plane.

Finally, the phase difference between two electron wave packets separated by an IR cycle is

$$\Delta\Phi_{k+1} + \Delta\Phi_k = -\frac{2W\pi}{\hbar\omega}. \tag{15}$$

The position of the maxima of the interference pattern due to superposition of the wave packets created in every cycle is given in this case by $W = n\hbar\omega$, where n is an integer. This expresses energy conservation and gives rise to interference circles centred at the origin.

4. Conclusions

In conclusion, we have studied the ionization of argon atoms by a train of attosecond pulses in the presence of a strong IR field as a function of the delay between the attosecond pulses and the IR field, using a velocity map imaging technique. The velocity maps exhibit interference patterns which strongly vary with the delay. We have used a simple analysis based on the strong field approximation to unravel the different interference structures observed. We find that one delay is particularly interesting: when the attosecond pulses coincide with the extrema of the IR vector potential, the initial momentum distribution gets shifted upwards and downwards for two consecutive attosecond pulses. As described in more detail in [5], the resulting interference pattern provides information on the phase variation of the initial momentum distribution, in a way analogous to lateral-shearing interferometry in optics.

Acknowledgments

We acknowledge the support of the Integrated Initiative of Infrastructure Laserlab-Europe (RII3-CT-2003-506350, FOSCIL), the Marie Curie Intra-European Fellowships (MEIF-CT-2004-009268, MEIF-CT-2003-500947), the Marie Curie Research Training Network XTRA

(MRTN-CT-2003-505138), the National Science Foundation through grant no 0401625, the Knut and Alice Wallenberg Foundation and the Swedish Science Council. The research of YN, FL, MFK and MJJV is part of the research program of the 'Stichting voor Fundamenteel Onderzoek der Materie (FOM)', which is financially supported by the 'Nederlandse Organisatie voor Wetenschappelijk Onderzoek (NWO)'. KV is on leave from the Department of Optics and Quantum Electronics, University of Szeged, Hungary.

References

[1] Kienberger R *et al* 2004 *Nature* **427** 817
[2] López-Martens R *et al* 2005 *Phys. Rev. Lett.* **94** 033001
[3] Dorner R, Mergel V, Jagutzki O, Spielberger L, Ullrich J, Moshammer R and Schmidt-Bocking H 2000 *Phys. Rep.* **330** 95–192
[4] Eppink A T J B and Parker D H 1997 *Rev. Sci. Instrum.* **68** 3477
[5] Remetter T *et al* 2006 *Nat. Phys.* **2** 323–6
[6] Aseyev S A, Ni Y, Frasinski L J, Muller H G and Vrakking M J J 2003 *Phys. Rev. Lett.* **91** 223902
[7] Bates W J 1947 *Proc. Phys. Soc.* **59** 940–52
[8] Mairesse Y *et al* 2003 *Science* **302** 1540
[9] Paul P M, Toma E S, Breger P, Mullot G, Augé F, Balcou P, Muller H G and Agostini P 2001 *Science* **292** 1689
[10] Varjú K *et al* 2005 *Laser Phys.* **15** 888–98
[11] Vrakking M J J 2001 *Rev. Sci. Instrum.* **72** 4084
[12] Johnsson P *et al* 2005 *Phys. Rev. Lett.* **95** 013001
[13] Lewenstein M, Balcou P, Ivanov M, L'Huillier A and Corkum P B 1994 *Phys. Rev.* A **49** 2117
[14] Quéré F, Mairesse Y and Itatani J 2005 *J. Mod. Opt.* **52** 339